NeuroImage 44 (2009) 870–883

Contents lists available at ScienceDirect

NeuroImage

journal homepage: www.elsevier.com/locate/ynimg

A study of diffusion tensor imaging by tissue-specific, smoothing-compensated voxel-based analysis

Jee Eun Lee [a,*], Moo K. Chung [a,b], Mariana Lazar [c], Molly B. DuBray [d], Jinsuh Kim [e], Erin D. Bigler [f,g,h,i], Janet E. Lainhart [f,d,h], Andrew L. Alexander [a,j,k]

[a] Waisman Laboratory for Brain Imaging and Behavior, Waisman Center, 1500 Highland Ave., Madison, WI 53705, USA
[b] Department of Biostatistics and Medical Informatics, University of Wisconsin, Madison, WI, USA
[c] Center for Biomedical Imaging, New York University School of Medicine, New York, NY, USA
[d] Interdepartmental Program in Neuroscience, University of Utah, Salt Lake City, UT, USA
[e] Radiology, University of Iowa, Iowa City, IA, USA
[f] Department of Psychiatry, University of Utah, Salt Lake City, UT, USA
[g] Department of Radiology, University of Utah, Salt Lake City, UT, USA
[h] The Brain Institute at the University of Utah, Salt Lake City, UT, USA
[i] Department of Psychology, Brigham Young University, Provo, UT, USA
[j] Department of Medical Physics, University of Wisconsin, Madison, WI, USA
[k] Department of Psychiatry, University of Wisconsin, Madison, WI, USA

ARTICLE INFO

Article history:
Received 13 December 2007
Revised 5 September 2008
Accepted 17 September 2008
Available online 11 October 2008

Keywords:
Diffusion tensor imaging
Smoothing
Voxel-based analysis
Autism

ABSTRACT

Voxel-based analysis (VBA) is commonly used for statistical analysis of image data, including the detection of significant signal differences between groups. Typically, images are co-registered and then smoothed with an isotropic Gaussian kernel to compensate for image misregistration, to improve the signal-to-noise ratio (SNR), to reduce the number of multiple comparisons, and to apply random field theory. Problems with typical implementations of VBA include poor tissue specificity from image misregistration and smoothing. In this study, we developed a new *t*issue-specific, sm*o*othing-compe*n*sated (T-SPOON) method for the VBA of diffusion tensor imaging (DTI) data with improved tissue specificity and compensation for image misregistration and smoothing. When compared with conventional VBA methods, the T-SPOON method introduced substantially less errors in the normalized and smoothed DTI maps. Another confound of the conventional DTI-VBA is that it is difficult to differentiate between differences in morphometry and DTI measures that describe tissue microstructure. T-SPOON VBA decreased the effects of differential morphometry in the DTI VBA studies. T-SPOON and conventional VBA were applied to a DTI study of white matter in autism. T-SPOON VBA results were found to be more consistent with region of interest (ROI) measurements in the corpus callosum and temporal lobe regions. The T-SPOON method may be also applicable to other quantitative imaging maps such as T1 or T2 relaxometry, magnetization transfer, or PET tracer maps.

Introduction

Diffusion tensor imaging (DTI) is a non-invasive imaging method for assessing the characteristics of tissue microstructure (Basser et al., 1994). DTI is very sensitive to changes in tissue microstructure changes, and thus is highly applicable to a broad spectrum of clinical and research applications. DTI data are acquired by measuring the apparent diffusivities in six or more non-collinear directions (Basser et al., 1994), and yield complex multi-variate measures of the diffusion tensor that describe the magnitude (trace and eigenvalues), the anisotropy (such as fractional anisotropy — FA), and the orientation (eigenvectors) of the apparent diffusivities. Measures of diffusion anisotropy, like FA, are small in gray matter (GM) and cerebral spinal fluid (CSF), reflecting nearly isotropic tensors, and are often much higher and heterogeneous in white matter (WM) (e.g., Alexander et al., 2007b). In general, the direction of greatest diffusivity within a voxel is assumed to be parallel to the predominant direction of the WM fiber bundles. FA in WM is likely to be modulated by a range of microstructural factors including myelination, axonal size and density, gliosis, neoplasia, edema and inflammation. However, FA is also modulated by partial volume averaging between WM and other tissues (GM and CSF) and intersecting fiber bundles at oblique angles (Alexander et al., 2001a). This heterogeneity in WM diffusion anisotropy necessitates the use of anatomically localized measurements for the analysis of DTI data.

There are several approaches for obtaining anatomically localized measurements in DTI data. Manual region-of-interest (ROI) methods

* Corresponding author. Fax: +1 608 262 9440.
E-mail address: jeelee@wisc.edu (J.E. Lee).

1053-8119/$ – see front matter © 2008 Elsevier Inc. All rights reserved.
doi:10.1016/j.neuroimage.2008.09.041

are appropriate for testing anatomically-specific hypotheses when the structure is easily defined (e.g., Alexander et al., 2007a; Bonekamp et al., 2007; Charlton et al., 2006; Gupta et al., 2006). Similarly, tractography methods have been used for extracting WM tract-specific regions for DTI analysis (Jones et al., 2006; Kanaan et al., 2006; Berman et al., 2005). Since ROI methods are usually applied in the original image space, the measurements are unaltered by additional image processing. However, ROI approaches including both manual tracing and tractography may introduce user selection biases and can suffer from poor consistency. Another widely used statistical image analysis approach is voxel-based analysis (VBA), which spatially normalizes (co-registers) the brain images across subjects and performs statistical tests at each voxel. The advantages of VBA are that it is highly reproducible, user-independent (for a specific algorithm), and it can explore differences over the entire brain without anatomically specific hypotheses. Potential limitations of VBA include poor image co-registration and weak statistical power from the large number voxels being tested. Despite these limitations, VBA has been widely used for DTI studies (e.g., Schmithorst et al., 2002, Schmithorst and Wilke, 2002; Hubl et al., 2004; Park et al., 2004; Tuch et al., 2005; Kumra et al., 2005; Snook et al., 2007; Xu et al., 2007; Albrecht et al., 2007; Borroni et al., 2007; Ardekani et al., 2007).

VBA methods for DTI data are not standardized, although most studies follow a procedure of spatial normalization, followed by spatial smoothing, voxel-based statistical testing, and statistical parametric mapping (SPM). Although advanced nonrigid image warping methods have been described for DTI VBA that reduce anatomical variability between subjects (Alexander et al., 2001b; Xu et al., 2003; Park et al., 2003; Zhang et al., 2006; Ashtari et al., 2007), these methods are not currently widely available for DTI analyses. Several DTI VBA studies reported using affine transformations for spatial normalization, which are widely available (e.g., AIR (Woods et al., 1998), FLIRT (Jenkinson and Smith, 2001) and SPM (Ashburner and Friston, 1999)), simple to implement, and generate anatomically similar maps in appearance (Jones et al., 2002; Schmithorst et al., 2002, Schmithorst and Wilke, 2002; Tuch et al., 2005; Salat et al., 2005; Jones et al., 2005; Whitcher et al., 2007; DaSilva et al., 2007). Other studies have used nonlinear transformations in SPM (e.g., Barnea-Goraly et al., 2003, 2004; Chappell et al., 2006; Snook et al., 2007) to improve the spatial normalization, although residual misregistration has been reported in the corpus callosum and near the cortex (Snook et al., 2007). Higher dimensional spatial normalization methods with elastic warping and large-scale diffeomorphic transformations have also been applied to DTI data and appear to have much higher spatial correspondence of white matter structures from different subjects (e.g., Park et al., 2003, 2004; Zhang et al., 2006; Ashtari et al., 2007; Ardekani et al., 2007). Regardless of the spatial transformation method, image warping can introduce additional partial volume averaging and smoothing into the image data sets, and may alter the distribution of the DTI measures in a region. Additionally, consistent differences in anatomical morphology can lead to misregistration errors that manifest as apparent differences in the DTI measurements. For example, FA and WM maps are similar, thus it is possible that statistically significant differences in the FA maps given by VBA may be caused by morphologic differences in the WM. Similarly, CSF and mean diffusivity (MD) maps are highly correlated, which makes MD differences around regions with CSF difficult to differentiate from morphology.

Spatial smoothing is a common step in VBA. The purpose of smoothing is multi-fold: (1) to reduce the effects of anatomic misregistration from poor spatial normalization, (2) to reduce noise and signal variations, and (3) to reduce the effective number of multiple comparisons in the statistical testing thus improving statistical power. However, spatial smoothing greatly increases the partial volume averaging of the DTI data. This means that signals from GM, WM, and CSF will be mixed together prior to the statistical comparison and statistically significant differences may arise from signals in any of the compartments in a region. Problems with partial volume averaging may be reduced by segmenting tissue types or regions prior to smoothing (e.g., Schmithorst et al., 2002, Schmithorst and Wilke, 2002; Albrecht et al., 2007; Grieve et al., 2007; Xu et al., 2007). Smoothing will subsequently cause the signals to blur near the edges of structures, which may result in systematic biases in the spatially blurred maps. For example, the FA values in WM will be reduced after blurring. The blurring bias will increase for either smaller structures or larger smoothing kernels.

This study addresses some of the potential problems with previous VBA studies by implementing a slightly modified VBA method. The first step is to segment the image data into tissue types – GM, WM and CSF – prior to spatial normalization to minimize further partial volume averaging and improve tissue specificity of the DTI measurements. The DTI maps and tissue masks are then spatially normalized to a brain template. Spatial smoothing is then applied to all normalized maps including the masks. Since the effects of spatial transformation and smoothing will be identical in all images including the processed DTI maps and WM mask, the effects of the spatial smoothing are compensated by dividing the smoothed DTI maps by the smoothed mask (also called the tissue density in voxel-based morphometry (Paus et al., 1999)). After all the image sets are processed in this manner, they are masked by a WM template that is defined by the average normalized WM mask at the 20% level. Statistical testing and parametric mapping are subsequently applied. This VBA procedure is called *ti*ssue-*spe*cific, sm*oo*thing-compe*n*sated (T-SPOON) VBA. Our prediction is that T-SPOON VBA will minimize the effects of partial volume averaging during the VBA processing. Also, since the effects of smoothing are compensated, the DTI measures in the normalized maps are more similar to those in the original data. Further, the smoothing compensation reduces the potential confound of the morphological differences.

In this study, the effects of T-SPOON processing were compared against conventional VBA both with and without prior WM segmentation. Specifically, the effect of spatial smoothing on the DTI maps was investigated. The VBA methods were also evaluated in a DTI study comparing measurements in autism versus typically developing controls. The VBA results were compared against published results obtained using manual ROIs in the corpus callosum and temporal lobe (Alexander et al., 2007a; Lee et al., 2007).

Methods

Subjects

DTI data from 77 male subjects were used in this study including 43 subjects with high functioning autism spectrum disorders [38 autism, 5 PDD-NOS (pervasive developmental disorder — not otherwise specified), mean age = 16.23 years, standard deviation = 6.70] and 34 control subjects matched for age (mean age 16.44, S.D. 5.97), handedness, IQ, and head size. More details about the subjects and related assessments are described in Alexander et al., (2007a).

DTI

DTI data were acquired on a Siemens Trio 3.0 Tesla Scanner with an 8-channel, receive-only head coil. DTI was performed using a single-shot, spin-echo, EPI pulse sequence and SENSE parallel imaging (undersampling factor of 2). Diffusion-weighted images were acquired in twelve non-collinear diffusion encoding directions with diffusion weighting factor $b = 1000$ s/mm^2 in addition to a single reference image (b 0). Data acquisition parameters included the following: contiguous (no-gap) fifty 2.5 mm thick axial slices with an acquisition matrix of 128x128 over a FOV of 256 mm, 4 averages, repetition time (TR) = 7000 ms, and echo time (TE) = 84 ms. Two-dimensional gradient

echo images with two different echo times of 7 ms and 10 ms were obtained prior to the DTI acquisition for correcting distortions related to magnetic field inhomogeneities.

Eddy current related distortion and head motion of each data set were corrected using an affine automatic image registration program (AIR, http://bishopw.loni.ucla.edu/AIR5/) and distortions from field inhomogeneities were corrected using custom software algorithms based upon the field map method described by Jezzard and Balaban (1995). Distortion-corrected DW images were interpolated to $2\times2\times2$ mm^3 voxels and the six tensor elements were calculated using a multivariate log-linear regression method (Basser et al., 1994). Then the tensor was diagonalized to estimate the three eigenvectors and the corresponding eigenvalues. Maps of the DTI FA and MD were subsequently calculated (Basser and Pierpaoli, 1996).

White matter segmentation

To minimize the effects of partial voluming between different tissue types, the white matter (WM) was first segmented using the *mFAST* algorithm (Zhang et al., 2001) in the FMRIB software library (http://www.fmrib.ox.ac.uk/fsl/). The segmentation algorithm was based upon a hidden Markov random field model and the expectation–maximization algorithm. The major ($\lambda1$) and minor eigenvalues ($\lambda3$) were used for the input channels in the *FAST* to generate the segmented WM maps. These two inputs appeared to be more robust and give more consistent segmentation results than any other combination of DTI measures. The binary WM mask was subsequently used to extract WM only maps of FA, MD and the three eigenvalues. WM voxels that bordered CSF appeared hyperintense in the MD maps, so voxels with MD values more than two standard deviations above the average MD for all cerebral WM were removed from the analysis. This approach minimized the effects of partial volume averaging artifacts that can be introduced during the subsequent spatial normalization and smoothing.

Template creation

The DTI data from a 16 year old control subject was used as an initial template data set. The segmented FA map for this subject was normalized to the MNI-152 white matter prior probability map using an affine transformation and mutual information for a cost function with 2 mm isotropic resolution over a 91x109x91 matrix. The FA maps for the other 76 subjects were spatially normalized to the single subject template set using a 12-parameter affine transformation with *FLIRT* (http://www.fmrib.ox.ac.uk/fsl/). The normalized FA maps were then averaged to create an average FA template.

Normalization

The FA maps for each subject were again spatially normalized to the average FA template using a 12-parameter affine transformation with *FLIRT* (http://www.fmrib.ox.ac.uk/fsl/). This secondary normalization step reduced the potential bias issues of using a single subject template. The same affine transformation was then applied to (a) the whole-brain (unsegmented) DTI maps (FA, MD, and eigenvalues), (b) the WM-segmented DTI maps, and (c) the binary WM mask maps. Trilinear interpolation was used to remap the image data in the normalized space. Normalized WM masks from all subjects were averaged to provide underlay images for display. The average WM mask was thresholded at the 20% level to restrict our results to probable WM regions in the normalized space.

Spatial smoothing

Isotropic Gaussian smoothing was applied to all the normalized image data (segmented and unsegmented). The smoothed, unsegmented maps are referred to as the 'UNSEG' datasets. The smoothed, segmented maps are referred to as the 'SEG' datasets.

Smoothing compensation

T-SPOON datasets were generated by dividing the SEG DTI maps by the SEG WM mask. Since the smoothed WM masks have the same blurring as the normalized and smoothed DTI maps, the division will make the smoothed data have values more similar to the original data set. The entire process is depicted in Fig. 1.

Smoothing compensation was also investigated as a function of the smoothing kernel size. Adverse smoothing effects were evaluated using a root mean squared error (RMSE) measure, which was defined as the root mean squared difference between signals in the smoothed VBA data and in the original unsmoothed data. This evaluation was performed for a single FA map with a range of Gaussian smoothing kernel widths (2–16 mm). The RMSE over the entire WM was investigated as a function of smoothing kernel width for all three VBA methods (SEG, UNSEG, and T-SPOON).

White matter voxel-based morphometry

The effects of morphometry on the VBA results were evaluated by performing voxel-based morphometry (VBM) analysis on the WM masks. The approach is similar to that described in the original VBM paper by Ashburner and Friston (2000). The WM density maps for each subject were defined by the smoothed, normalized WM masks. The effects of T-SPOON smoothing compensation on VBM were also evaluated by dividing the smoothed WM masks by the same map. We hypothesize that, at least within the average WM mask volume, the smoothing compensation will remove the morphologic edge effects that will confound standard VBA methods. Voxel-based statistical testing was performed on the WM density maps (described in next sub-section).

Multi-subject statistics — application to autism

Results from voxel-based ANCOVA between autism and control groups were used to compare different VBA methods as well as the results of WM VBM. Age was used as a covariate. Gaussian smoothing kernel sizes between 0 mm (no smoothing) and 16 mm were investigated. Statistical analyses were performed using the software package FMRISTAT (http://www.math.mcgill.ca/keith/fmristat/). Analyses were restricted to regions in the average WM mask that were above the 20% threshold. The specific statistical threshold was varied depending upon the specific evaluation being performed.

Results

Quantitative assessment of individual subject data for smoothing compensation of T-SPOON

The effects of smoothing on FA maps processed using UNSEG, SEG and T-SPOON methods are illustrated in Fig. 2a. These maps show the RMSE between FA values in the smoothed maps and original map. As expected, both the SEG and UNSEG methods show considerable errors, particularly at the interfaces with other tissues, with the SEG map being the worst. Conversely, T-SPOON processing introduces the least RMSE with increased smoothing. Inspection of the error maps not only demonstrates that the errors are larger in the SEG and UNSEG maps, but the amount of error is quite heterogeneous over the WM, which may adversely affect the statistical analysis. The T-SPOON map errors are largest in heterogeneous WM regions (e.g., near the cingulum bundles and corpus callosum, and in the centrum semiovale in Fig 2a), which is an issue for any smoothing method as fine details will be 'washed out'. However, it is also obvious, that the

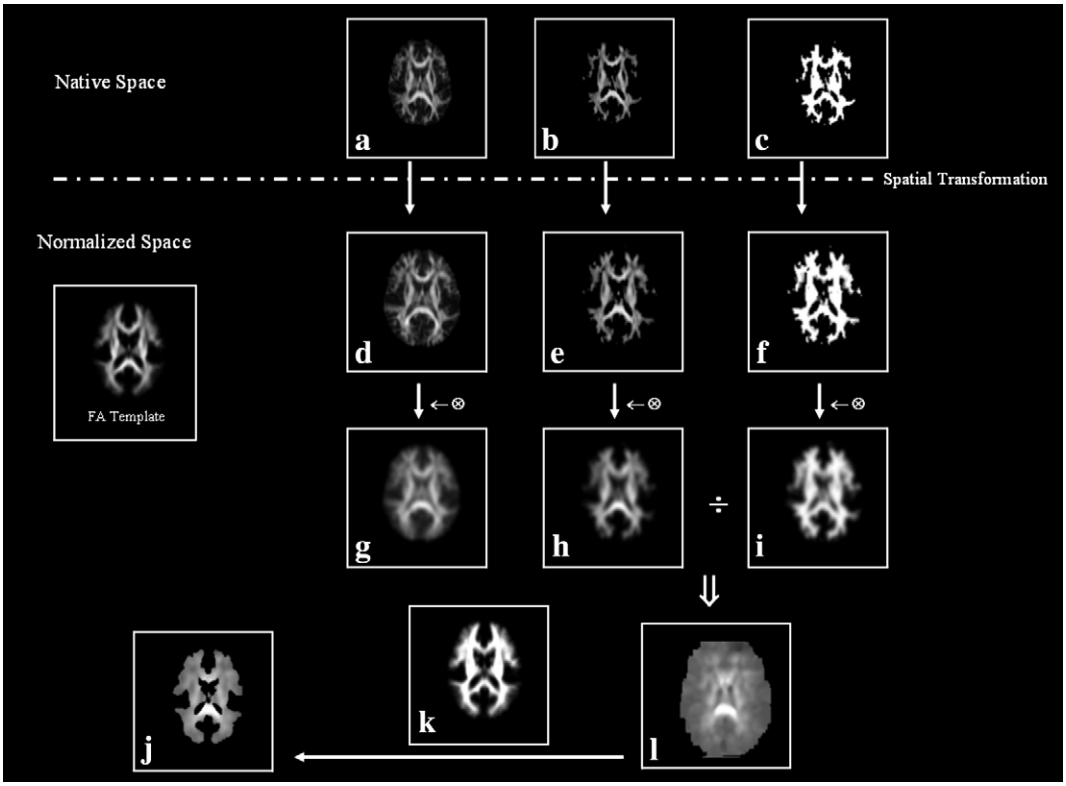

Fig. 1. Flow diagram/example of the processing steps for T-SPOON data for a subject. The main steps are (1) segmentation of the WM, (2) spatial normalization of all maps including the WM mask, (3) spatial smoothing with Gaussian kernel, (4) division of the smoothed, normalized DTI data by the smoothed, normalized WM mask, and (5) mask corrected data by WM mask defined by the average WM template. a: original FA map; b: white matter segmented FA map; c: binary WM mask; d: normalized FA map; e: normalized WM segmented FA map; f: normalized WM mask; g: UNSEG — smoothed, normalized FA map; h: SEG — smoothed, normalized, segmented FA map; i: smoothed, normalized WM mask; j: masked T-SPOON FA map; k: average of normalized white matter mask; l: T-SPOON FA map (no masked map).

T-SPOON errors in these regions are smaller than the other approaches. The average RMSE of smoothed FA maps versus smoothing kernel size within all WM voxels in the brain is plotted in Fig. 2b. Fig. 2c shows a toy simulation of a narrow rotated signal phantom both with and without T-SPOON. In this simple example, the signal interpolation following phantom rotation by 45°causes a large drop in the signal intensities. The original signal levels are nearly restored following T-SPOON correction. From both of human brain FA data and the simulation, it is clear that T-SPOON introduces the least error. Note that smoothing will introduce some error regardless of whether or not it is specific to WM since the FA is heterogeneous. Investigation of errors in the other maps (e.g., MD and eigenvalues) shows similar error patterns although the SEG method is much worse than the other two approaches (data not shown). The worse performance for the SEG method is caused by the increased partial volume effects between WM and zero signal, which is larger than the signal differences between WM and either GM or CSF.

The effects of morphology on VBA

A voxel-based autism versus control group comparison of FA and MD maps was performed using ANCOVA with age as a co-variate. The statistically significant areas are shown in Fig. 3 and Fig. 4. The color bars represent the range of *t*-values. Voxel-based morphometry (VBM) was also performed using the WM masks for both the SEG and T-SPOON methods. An 8 mm smoothing kernel was used, and the statistical maps were thresholded using an uncorrected $p<0.05$. This low statistical threshold was used to demonstrate the potential confounds of VBA associated with morphology, and not for specific interpretation. Close inspection of the FA SEG and WM SEG VBM maps demonstrates similar regions of significant signal difference in both sets of analyses. These results suggest that the observed FA differences may be caused by either the morphology or the inherent FA of the tissue in the region. The T-SPOON and UNSEG data show more diffuse regions of FA group differences than the SEG map although some of the regions correspond to the WM SEG VBM regions. The T-SPOON analysis of WM VBM does not show any significant differences in morphometry after the smoothing correction is performed, thus it is not a significant confound in the FA T-SPOON results. Note that many of the significantly different regions are similar for both T-SPOON and either UNSEG or SEG FA analyses, yet it was unclear whether the FA map differences with SEG or UNSEG were caused by the morphometry effect.

Effects of the smoothing kernel width

The effects of the smoothing kernel width were examined for a range between 0 mm and 16 mm. The results for UNSEG and T-SPOON analyses are shown in Fig. 5 as well as the results from WM VBM with the same smoothing kernels for a single coronal slice in the middle of the brain. Many of the significant UNSEG FA regions are also significant for the UNSEG WM VBM results (Figs. 5a and b), thus the confounding effects of morphology cannot be ruled out. The T-SPOON FA results show similar regions to the UNSEG FA analysis; however, the confounding effects of morphology have been removed (bottom row Figs. 5a and b). In this case a smoothing kernel of 10 mm or more appears to show significant effects in nearly all the same areas for T-SPOON FA VBA except in the bilateral cingulum bundles in the temporal lobe. Significant group FA differences in the bilateral temporal stem were only observed with at least 10 mm of smoothing. The effects of smoothing on MD VBA are shown in Figs. 5c and d. A few

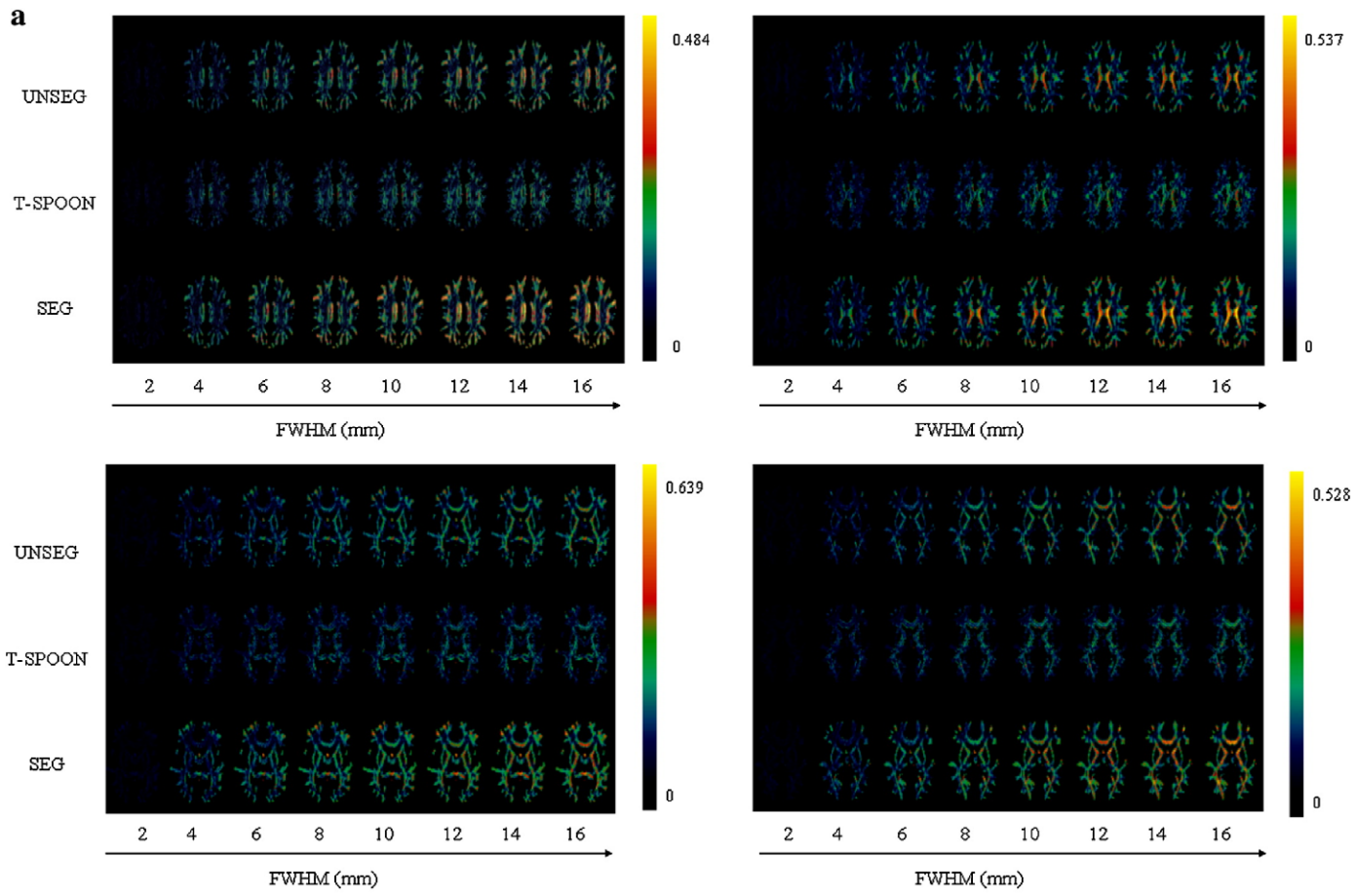
a
UNSEG
T-SPOON
SEG
0.484
0
0.537
0
2 4 6 8 10 12 14 16
FWHM (mm)
UNSEG
T-SPOON
SEG
0.639
0
0.528
0
2 4 6 8 10 12 14 16
FWHM (mm)

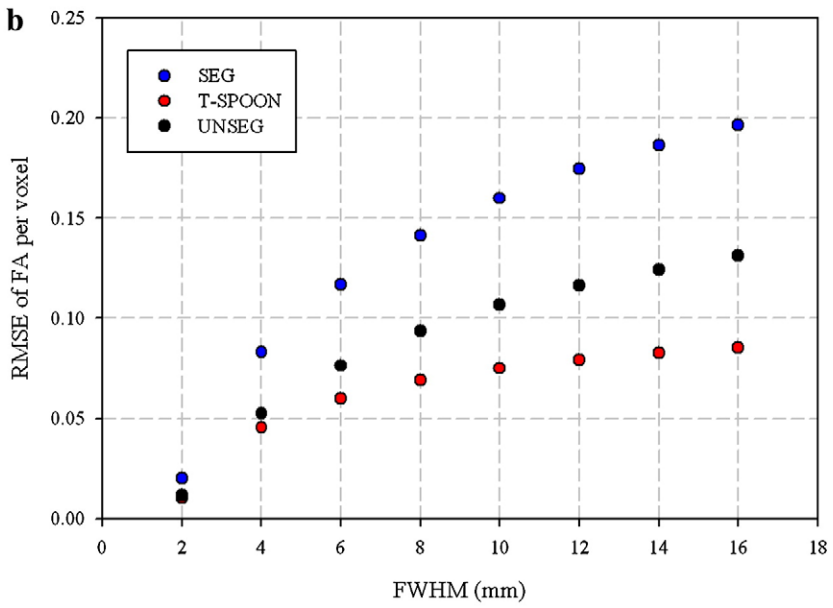
b
SEG
T-SPOON
UNSEG
RMSE of FA per voxel
0.25
0.20
0.15
0.10
0.05
0.00
0 2 4 6 8 10 12 14 16 18
FWHM (mm)

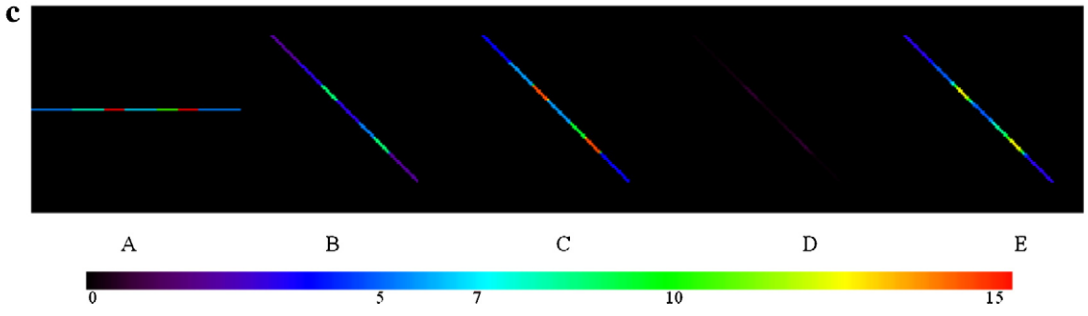
c
A
B
C
D
E
0
5
7
10
15

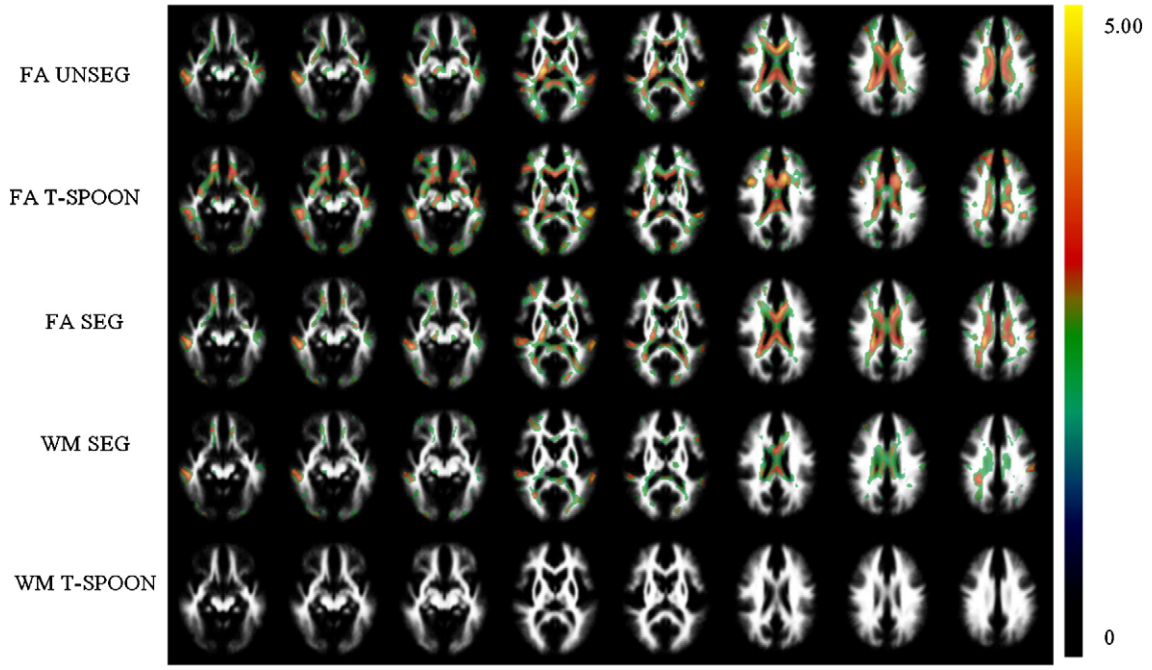

Fig. 3. Effects of WM morphology on FA group differences. The smoothing kernel width was 8 mm and the statistical threshold was an uncorrected $p<0.05$. The color corresponds to the *t*-statistic level. The three VBA approaches show similar regions with statistically significant decreased FA in autism although the effects are larger for the UNSEG and T-SPOON analyses. A voxel-based morphometry (VBM) study of the WM masks from the same data (WM SEG results) demonstrated reduced WM densities in the autism group in some of the same areas that were statistically significant in the FA VBA results. This makes it difficult to assess whether the VBA differences indicate effects from FA or morphology. The T-SPOON processing removed the WM morphometry effects, so the results are less ambiguous (see WM T-SPOON results).

regions of significant morphologic effects are observed although the extent does not closely match the MD VBA results. The UNSEG MD and T-SPOON MD VBA analyses both show extensive regions of group differences with some similarities. One important difference is that the UNSEG MD VBA is not significant in the corpus callosum except for very large smoothing kernels. In contrast, the T-SPOON MD VBA shows significant group differences in corpus callosum with 4 mm of smoothing or more, and also shows more extensive group differences in temporal lobe and temporal cingulum bundle regions.

Evaluation of Gaussian residuals

The evaluation and interpretation of voxel-based statistical testing is most straightforward when the samples are normally distributed with respect to the statistical model. The Bera–Jarque hypothesis test of composite normality of the residuals from the voxelwise ANCOVA for FA and MD is mapped in Fig. 6 (a and b, respectively) for a range of different smoothing kernel sizes (0 to 16 mm). The UNSEG and SEG VBA of FA show similar regions with non-Gaussian residuals and do not appear to improve much with larger smoothing kernels. In contrast, the extent of non-Gaussian residuals does significantly reduce with more smoothing for T-SPOON FA VBA. The non-Gaussian residuals are much more extensive in the MD VBA studies and again smoothing does not reduce this effect much for the UNSEG MD VBA. T-SPOON with some smoothing does appear to reduce the amount of non-Gaussian residuals. One potential reason that T-SPOON appears effective in reducing the non-Gaussian residuals is that the correction effectively normalizes the signal intensities of blurred data. While smoothing decreases the effects of misregistration, the signals in the tails of the smoothing kernel are much less than at the center. T-SPOON compensates for the signals at the tails of the smoothing kernel.

Group comparison results with different VBA approaches

Fig. 7 contains maps of statistically significant differences for FA and MD for both the UNSEG and T-SPOON methods. A 10 mm Gaussian smoothing kernel was used. To reduce the effects associated with multiple comparisons, a False Discovery Rate (FDR) threshold of 0.025 was used in combination with cluster extent criterion of $p<0.05$. The color bars in Fig. 7 represent the range of *t*-values. The highlighted regions demonstrate significantly decreased FA and increased MD in the autism group. There were no regions of significantly increased FA or decreased MD in the autism group. The FA results appear similar for both UNSEG and T-SPOON and include regions of the corpus callosum and bilateral superior temporal gyrus which were shown to be significantly different using region-of-interest measurements (Alexander et al., 2007a; Lee et al., 2007) and in addition, anterior cingulate WM. The MD statistical map showed more diffuse regions of group differences in the T-SPOON map. Again, statistically significant differences were observed in the corpus callosum, superior temporal gyrus, and temporal stem, which are consistent with analyses obtained using ROI methods (Alexander et al., 2007a; Lee et al., 2007). In addition, the T-SPOON analysis of MD data showed significant group differences in the thalamic, orbito-frontal, dorso-medial frontal, posterior cingulate, and occipital WM. Group analysis of the SEG

Fig. 2. The effects of spatial smoothing an FA map for different voxel based analysis approaches. (a) The maps show the root mean squared error (RMSE) between the smoothed map and the original unsmoothed data. The T-SPOON method demonstrates much less error as a function of the smoothing. SEG = segmented WM data. UNSEG = unsegmented WM data (e.g., whole brain). (b) Plots of the total integrated RMSE for the maps in (a). These results clearly demonstrate that T-SPOON reduces the errors introduced by spatial smoothing. The SEG approach introduces the most error. (c) 'Toy' simulation: (A) The original phantom is a horizontal line segment with variable intensities. (B) The phantom was rotated 45 degrees, which caused the phantom intensities to drop following the interpolation with the background. (C) After T-SPOON correction the phantom intensities are much more similar to the original. (D) The rotated phantom in B was smoothed with an isotropic Gaussian kernel and the intensities are reduced further. (E) The application of T-SPOON to the smoothed, rotated data restores much of the original signal pattern although it is blurred by the smoothing across the phantom. The color bar indicates the signal intensities in the simulation phantom.

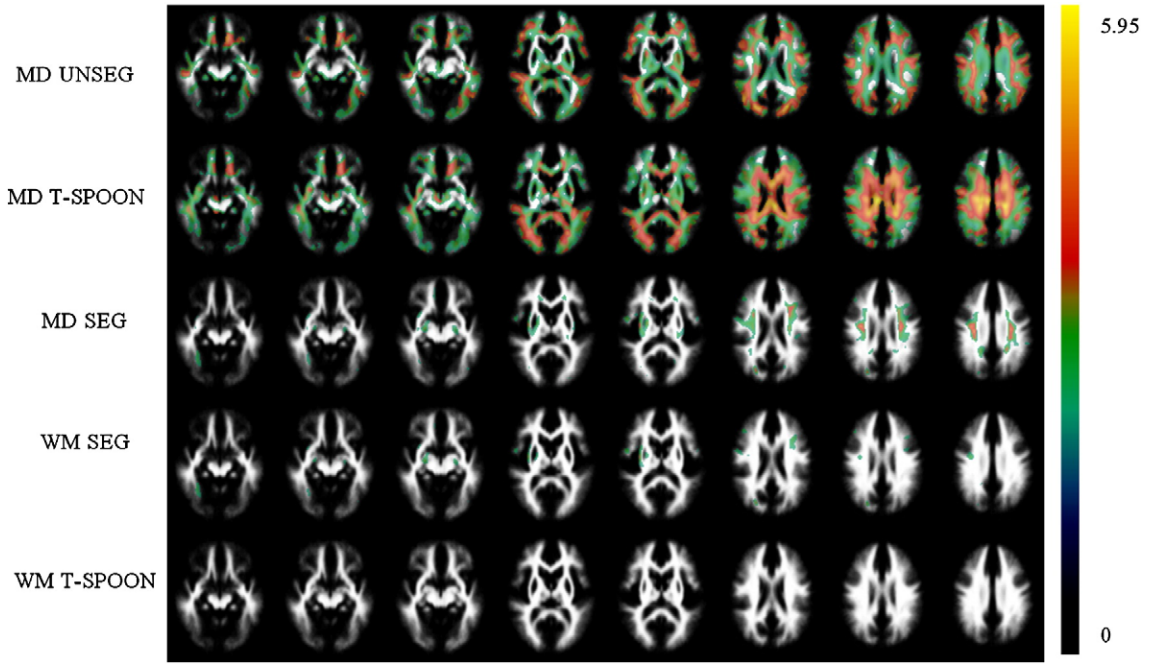

Fig. 4. Effects of WM morphology on MD group differences. The smoothing kernel width was 8 mm and the statistical threshold was an uncorrected $p<0.05$. The color corresponds to the *t*-statistic level. The UNSEG and T-SPOON VBA approaches show diffuse regions with statistically significant increased MD in the autism group. The SEG VBA results show much less differences. A voxel-based morphometry (VBM) study of the WM masks from the same data (WM SEG results) demonstrated increased WM densities in the autism group in some of the same areas that were statistically significant in the MD VBA results, particularly for the SEG analysis. Similar to Fig. 3, the T-SPOON processing removed the WM morphometry effects, so the results are less ambiguous (see WM T-SPOON results).

data for either FA or MD did not reveal any regions with statistically significant differences. The analyses were also repeated without age as a covariate and the results were similar. Given the broad age range of subjects in this study, we decided to present the data with age as a co-variate to reduce effects from age related changes. Detailed future studies will be necessary to better characterize the age related changes of DTI measures in autism and compare those against other developmental groups.

Correlations with processing speed in autism

In a recent study of DTI in the corpus callosum in these subjects (Alexander et al. 2007a), a speed of processing behavioral measure based on the Wechsler Processing Speed Index (Digit Symbol-Coding and Symbol Search subtests) was found to be positively correlated with FA (significant in the genu: $p=0.014$) and negatively correlated with MD (significant in total corpus callosum: $p=0.027$; splenium: $p=0.032$; and approaching significance in the genu and the body) in a group of 21 autistic subjects. A voxel-based correlation analysis of the same autistic subjects and the Wechsler Processing Speed Index was performed using each of the VBA methods. A statistical threshold of $p<0.05$ (uncorrected) was used to assess statistical significance. The SEG method did not reveal any significant correlations. Fig. 8 summarizes the FA and MD VBA results in a mid-sagittal section of the corpus callosum for both UNSEG and T-SPOON VBA. The T-SPOON method, but not UNSEG VBA revealed negative correlations between processing speed and MD in diffuse corpus callosum regions, which was consistent with the previously published results (Alexander et al., 2007a). T-SPOON VBA of FA versus processing speed also showed significant correlations in the genu, which was also consistent with the published ROI results (Alexander et al., 2007a); however, the UNSEG VBA did not demonstrate significant differences in this region. Conversely, both UNSEG and T-SPOON VBA methods also found significant focal regions in the body of the corpus callosum in the FA versus processing speed test, which were not observed in the published study (Alexander et al., 2007a).

Discussion

In this paper, we describe a correction method, T-SPOON, for reducing the partial volume effects of image registration and smoothing on DTI voxel based analyses. The method uses a region mask, in this case WM, to generate maps of the partial volume effects so that the data values will be renormalized after the smoothing operation. An investigation of the effects of smoothing on voxel-based analysis methods demonstrated that T-SPOON resulted in the least change in the actual image values. This means that smoothed images processed with T-SPOON will have intensity values more similar to the original data in the native space. This will not necessarily be the case for images processed using smoothed, segmented (SEG) or smoothed, unsegmented (UNSEG) methods since the smoothing will mix the signals from both within and outside the region. In this study, we specifically examined total cerebral WM, which was segmented from other tissues. The approach will be equally applicable to other tissues (e.g., GM, although this will have higher inherent partial volume effects with CSF near the cortex), regions or image contrasts. For example, the technique would be applicable to a restricted anatomical region like the corpus callosum which could be segmented for all subjects and spatially normalized. Furthermore, T-SPOON would also be applicable to other quantitative image contrasts like T1 or T2 relaxometry maps or PET tracer studies.

It should be noted that the results are dependent upon the region segmentation, particularly if the measurements are heterogeneous. In this study, we used eigenvalue maps of $\lambda 1$ and $\lambda 3$ to segment WM. This appeared to generate maps that were consistent with known WM although this was not rigorously evaluated. One obvious 'problem' region in the segmentation was the thalamus, which contains axons and is more similar to WM than other GM regions. Portions of the thalamus were often segmented and included in the WM. Other segmentation approaches could also be employed including the use of a co-registered T1-weighted image or other structural images for segmentation. Obviously, this

requires the DTI study to be exactly registered with the structural images. It should be noted that brain image segmentation is always somewhat problematic since there is no gold standard. Regardless, improvements to image segmentation and more anatomically specific segmentation will further improve the results generated using T-SPOON.

The T-SPOON approach mitigates the effects of morphologic effects caused by anatomic misregistration. For example, a WM mask and an

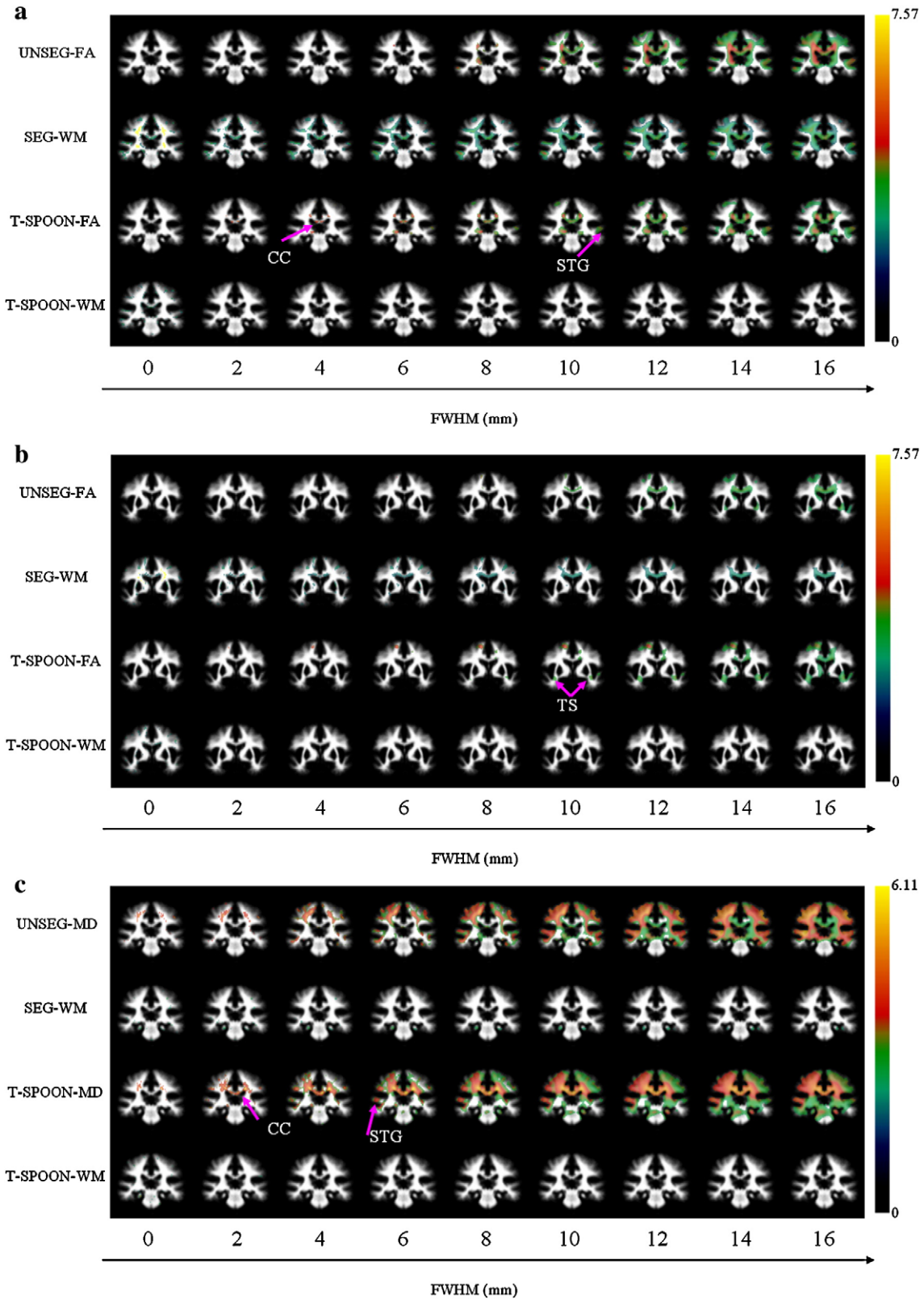

Fig. 5. The effects of the smoothing kernel width (0 to 16 mm) on group comparisons (autism versus controls) of FA (a and b) and MD (c and d) data for two coronal slices. As a statistical threshold, an uncorrected $p<0.05$ was used for the WM morphometric analysis and an FDR<0.025 and a cluster extent criterion of $p<0.05$ for FA and MD analyses. Images labels are CC: Corpus callosum; STG: superior temporal gyrus white matter; TS: temporal stem.

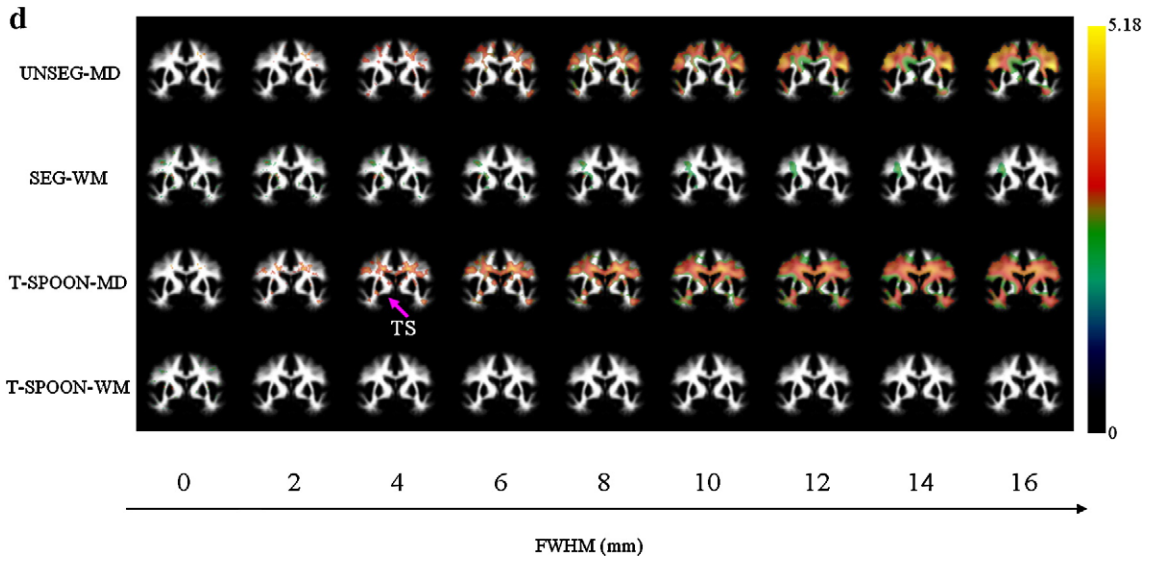

Fig. 5 (*continued*)

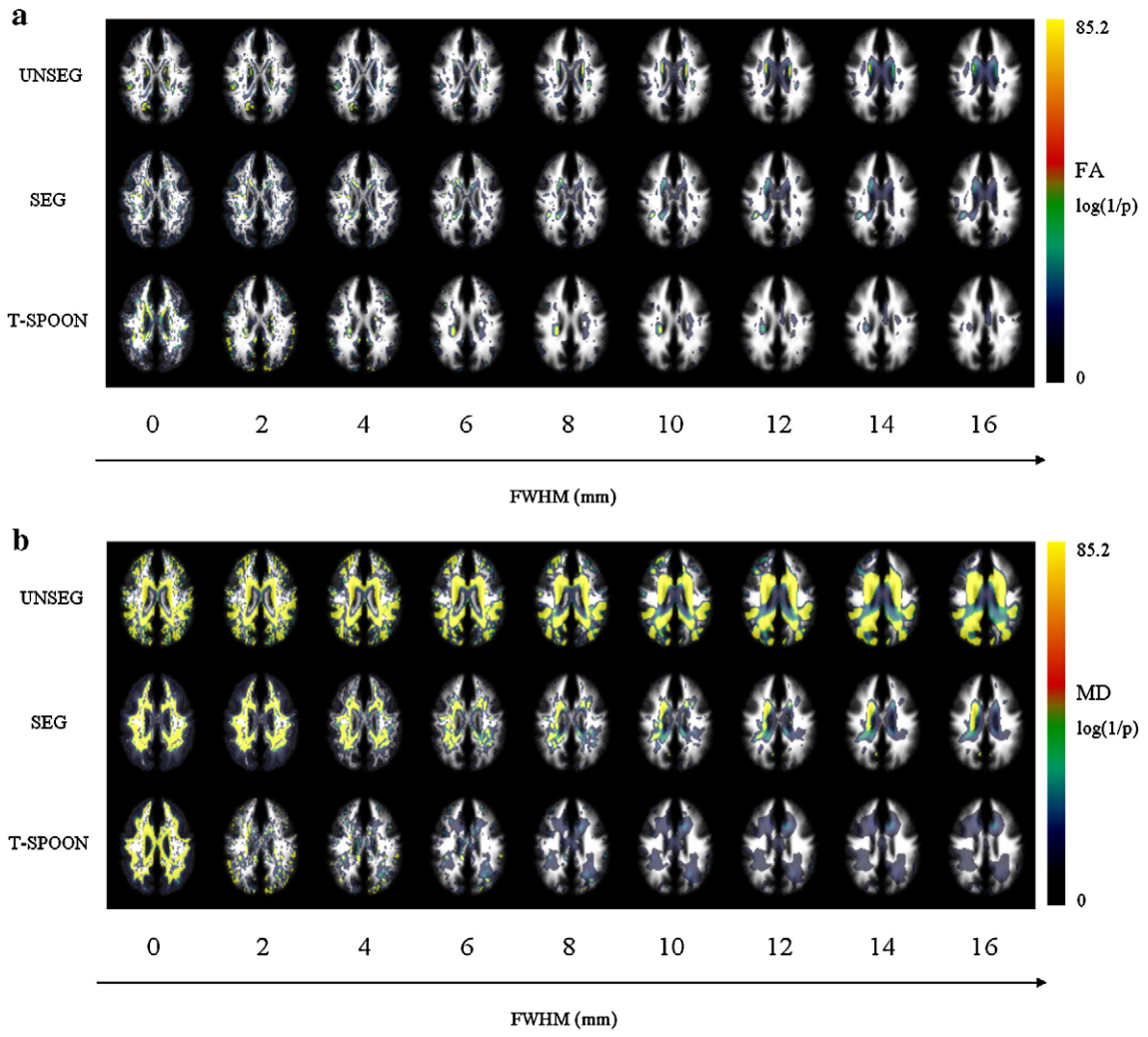

Fig. 6. Maps of voxels with non-Gaussian residuals as a function of the VBA method and smoothing kernel width. Colored voxels indicate non-Gaussian residuals at a significance level of $p<0.05$, and the natural logarithm of the p-value from the Bera–Jarque test was mapped corresponding to the color bar. If the p-value was 'zero' then p was assigned to be 1e 37, which led to 85.2 for the maximum log (p). (a) is for voxels with non-Gaussian residuals from ANCOVA for FA, and (b) for MD.

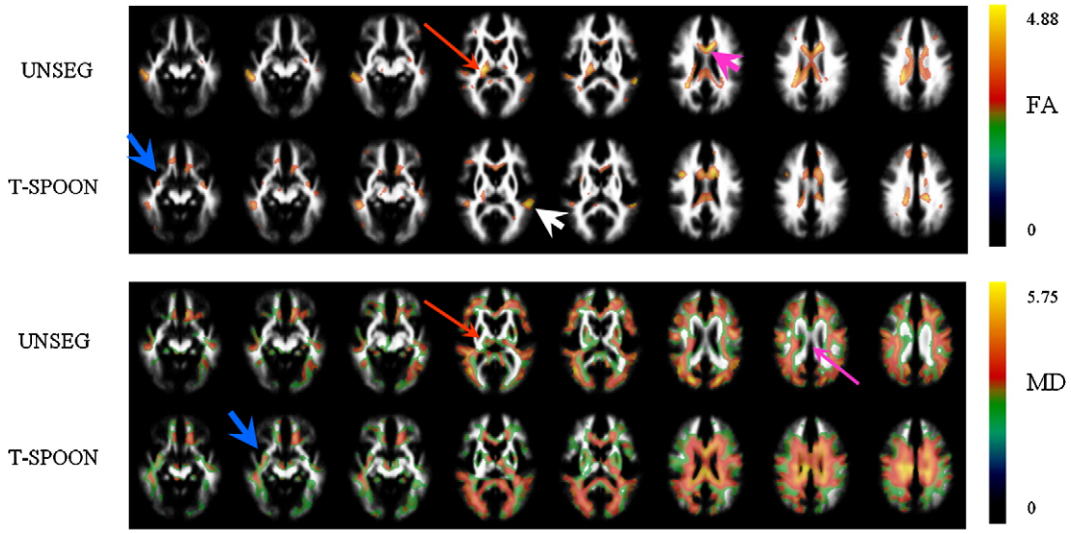

Fig. 7. Group comparisons (autism versus controls) of FA and MD data. The smoothing kernel width was 10 mm. False positive errors from multiple comparisons were reduced using an FDR<0.025 and a cluster extent criterion of $p<0.05$. The SEG VBA results were not statistically significant for either FA or MD at the threshold that was used in this figure. Group comparisons found significantly reduced FA for both UNSEG and T-SPOON VBA in the superior temporal gyrus WM, the thalamus and the corpus callosum. The temporal stems were only detected by T-SPOON VBA The autism group showed significantly increased MD in both the UNSEG and T-SPOON VBA maps. Of particular interest, the T-SPOON method found large group differences in the corpus callosum (consistent with Alexander et al., 2007a) also in the temporal stems, whereas the UNSEG method did not. Otherwise both UNSEG and T-SPOON demonstrated similar regions of significant differences. Colored arrows point to red: thalamus; pink: corpus callosum; blue: temporal stem; white: superior temporal gyrus white matter.

FA map appear quite similar, thus significant differences may be caused by either differences in morphology or FA particularly at the edges of the WM mask. The combination of blurring and correction with T-SPOON greatly reduces the local effects of morphologic differences, particularly when the normalized WM template mask is used. For example, if the WM is consistently narrower in one group, but the FA values are nearly identical, standard methods may detect significant differences in FA caused by the differences in morphology. The smoothing compensation of T-SPOON will remove the morphologic effects in this case, which will yield a null result. However, the method does not completely eliminate the effects of image misregistration, particularly if the image values in a region are heterogeneous. For example, if structure A (high FA WM region) for one group consistently overlapped with structure B (low FA WM region) for the other group, then that may yield a false difference. Conversely, if the signals in a region or across regions are uniform, then more misregistration could be tolerated. One potential weakness with the study is the use of affine spatial normalization, which has limited accuracy of anatomic co-localization. Recent development of advanced image registration algorithms including nonlinear warping approaches should improve the anatomical correspondence of normalized DTI data, which will likely improve multi-subject VBA

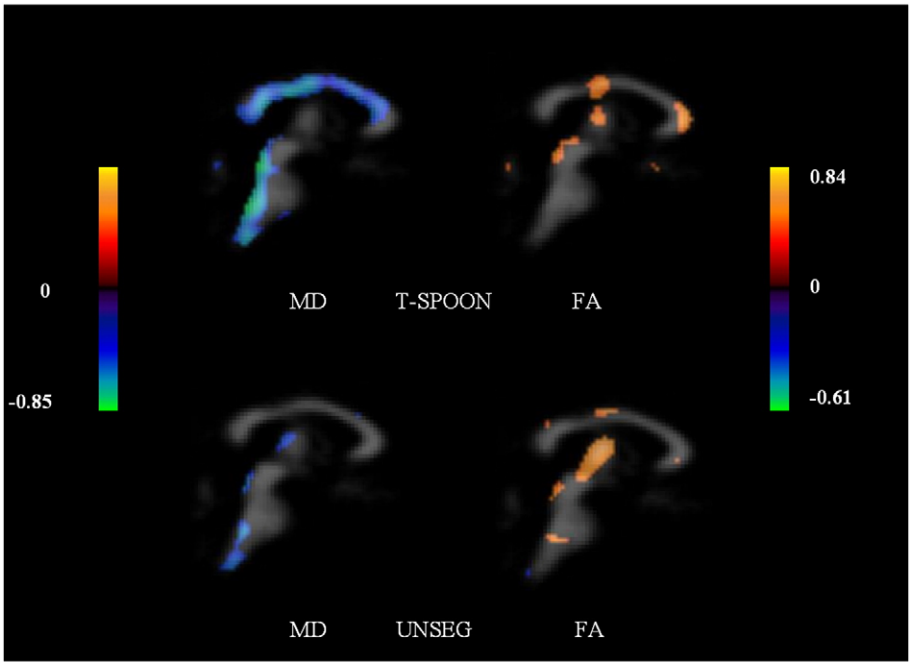

Fig. 8. Correlation maps of the processing speed index versus MD and FA in the mid-sagittal plane of the corpus callosum in a group of 21 autistic subjects. Significant positive correlations with FA were observed in the body for both T-SPOON and UNSEG VBA; whereas the T-SPOON also showed a region in the genu. Significant negative correlations with MD were observed in several corpus callosum regions using the T-SPOON method, but were not observed for the UNSEG method. The SEG VBA method did not reveal any significant correlations.

(Alexander et al., 2001b; Xu et al., 2003; Park et al., 2003; Ardekani et al., 2004; Zhang et al., 2006; Ashtari et al., 2007; Avants et al., 2007). However, there are no standard nonlinear warping methods and they are not currently widely available. Even in the case of perfect anatomic registration, spatial interpolation from image normalization and spatial smoothing will introduce partial volume averaging in the normalized data, which may be compensated using T-SPOON.

The primary validation for our current study is the comparison of results from our published regional data (Alexander et al., 2007a; Lee et al., 2007). In those studies, significant differences were observed in the corpus callosum as well as temporal lobe WM regions (superior temporal gyrus WM and temporal stem). The T-SPOON VBA of MD and FA showed significant group differences in all of these regions. Furthermore, voxel-based correlation analysis between DTI measures and processing speed data in 21 autism subjects with T-SPOON VBA showed statistically significant correlations in the corpus callosum. One of the main applications of VBA is to perform exploratory analyses of group data; therefore, it is reassuring that the T-SPOON VBA of DTI data showed consistent regions of statistical significance to previous region-specific analyses.

Direct comparisons between region-of-interest and VBA of DTI data have only been performed in a limited number of studies. Snook et al. compared manual ROI analysis with VBA using SPM (Snook et al., 2007). In their study, they concluded that the ROI analysis and VBA methods resulted in comparable findings, however, potential problems of the methods included the limitations of spatial normalization in VBA (particularly in the splenium of the corpus callosum) and massive averaging effects with the manual ROI analysis. Manual ROI validation was also noted in the paper (Kubicki et al., 2002). After VBA, the significant clusters may be inversely transformed to the native data for each subject for confirmatory ROI analysis. This would enable both the validation of the measurements in the original data space and the anatomical consistency of the regional measurements.

In this study, we explored the effects of the smoothing kernel size (0–16 mm) on the statistical maps for T-SPOON, UNSEG and SEG methods. It is known to have significant effects on the results of VBA of DTI data (Jones et al., 2005). For all smoothing kernel sizes, significant differences were not observed for the SEG method suggesting that this is not a good approach for VBA. Larger clusters were often observed with less smoothing using T-SPOON (i.e., MD and FA with 4 mm smoothing). In general, the regions of significant differences using T-SPOON did not change much as the smoothing kernel was increased above 10 mm. T-SPOON is likely to demonstrate similar behavior with smoothing which would predict that the optimum filter kernel width should be similar to the expected extent of the signal difference (e.g., the matched filter principle). Smoothing can be useful for decreasing the signal variance in a region from poor SNR; however, it can also smooth out critical features like a lesion or a small WM tract, which is clearly undesirable. In particular, smoothing may obscure regional differences in WM FA, which can be quite heterogeneous. The problems of over-smoothing are similar to any region-of-interest based analysis method as VBA is essentially a method for evaluating many regions-of-interest simultaneously. Smoothing also decreases the effective dimensionality of an image which is helpful for reducing the number of multiple comparisons in statistical testing, thereby increasing statistical power. Note that T-SPOON does not alter smoothed signals deep within large regions. It only compensates for the effects of smoothing near region boundaries. Thus, blurred regions with heterogeneous FA will suffer from decreased anatomical specificity. Smoothing will extend signals outside the WM mask boundaries, which may appear undesirable. However, the T-SPOON smoothing compensation will make the smoothed WM signals outside the original WM boundary similar to those within the WM region. Another important consideration for the smoothing kernel width is the expected amount of anatomical misregistration. If anatomical structures are accurately co-registered, then less smoothing may be required. However, in cases of poor registration, larger smoothing kernels are necessary to guarantee the overlap of specific structures. The obvious cost of increased smoothing is a reduction of anatomic specificity as large smoothing kernels increase the likelihood that multiple structures are included in the kernel width. In our study the UNSEG and T-SPOON methods demonstrated similar spatial patterns of group differences, though there were important differences. The T-SPOON MD results show significant differences in the corpus callosum with as little as 2 mm of smoothing, whereas at least 10 mm so smoothing were necessary for the UNSEG VBA and the differences were not as significant.

The statistical testing was limited to regions in the average WM map template with a 20% threshold, which was selected arbitrarily. The main effect of this thresholding was to reduce the spurious effects at the edges of the WM and more importantly to reduce the effects of multiple comparisons. The threshold could have been increased further, which would increase statistical power at the expense of losing finer WM structures, particularly at the brain periphery.

The smoothing compensation in T-SPOON bears some similarities to a VBA approach recently proposed by Oakes et al., (2007), which

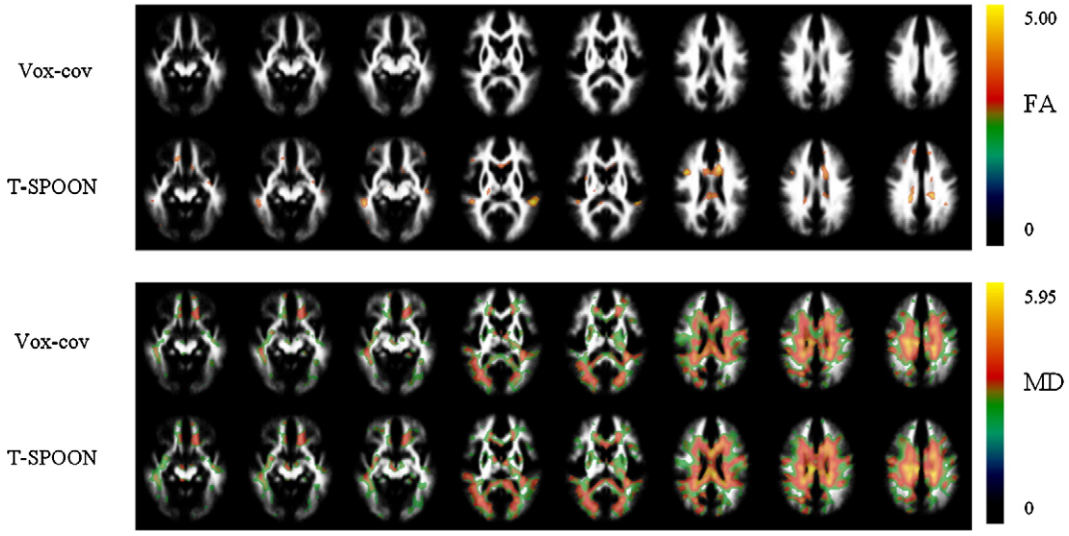

Fig. 9. Group comparisons (autism versus controls) of FA and MD data using the covariate method (Vox-cov) and T-SPOON. The smoothing kernel width was 8 mm. False positive errors from multiple comparisons were reduced using an FDR<0.025 and a cluster extent criterion of $p<0.05$. The covariate method VBA results were not statistically significant for FA at the threshold that was used in this figure. The results of the MD group comparison were similar between two methods.

includes the tissue probability map (in this case, the smoothed WM mask) as a covariate in the general linear model (GLM). The main difference is that the co-variate approach weights the smoothed data according to the partial volume effects in the statistical analysis, whereas the T-SPOON method compensates for the smoothing prior to statistical analysis and therefore the compared images should have values more similar to the original data. The results using T-SPOON were compared against those from the covariate method (see Fig. 9). The results of the MD group comparison were similar between the covariate method and the T-SPOON approach; however, the FA group comparison did not show any significant differences using the covariate method, whereas T-SPOON showed significant differences in the corpus callosum, superior temporal white matter, and ventral prefrontal white matter regions. Thus, the T-SPOON FA tests were more consistent with previously published studies using ROI based approaches (Alexander et al., 2007a; Lee et al., 2007). Lowering the statistical threshold from FDR<0.025 to FDR<0.05 yielded more similar group FA difference maps between the covariate and T-SPOON approaches. Thus, we believe that including the tissue probability map in the model decreases the degrees of freedom which weaken the statistical power of the analysis although the covariate method is still effective for removing the partial volume effects from normalization and smoothing.

The application of VBA for the analysis of DTI image data has been viewed by many as being somewhat controversial for many of the reasons that have been discussed above (registration, segmentation, partial volume effects, morphometry confounds, etc.). The issues of VBA are nicely illustrated in a recent study by Jones et al. (2007), which compared VBA results of the same data by several research groups who analyzed the data using different VBA approaches with differences in the spatial normalization method, the spatial filter size, the statistical testing (parametric versus nonparametric) and statistical thresholds. Similarly, the results of this study demonstrated inconsistency between different VBA methods. The T-SPOON method described in this paper will reduce the effects of spatial smoothing that result from spatial normalization and Gaussian kernel smoothing. However, T-SPOON does not completely resolve all of the analysis protocol differences discussed in the Jones study. Further improvements to algorithms for image co-registration and segmentation of DTI data will likely improve VBA. The selection criteria for statistical testing methods and thresholding are important considerations which will influence the interpretation of the results. Regardless of the VBA method, the analysis should be viewed as exploratory and careful validation is recommended. Furthermore, even if a region is not found significant using VBA, a more detailed analysis using anatomically specific ROIs will be more sensitive and may detect differences that are missed using VBA.

Recently, alternative strategies to whole brain DTI analysis have been proposed including Tract Based Spatial Statistics (TBSS — Smith et al., 2006), tractography based segmentation (e.g., Xue et al., 1999, Conturo et al., 1999; Basser et al., 2000; Lazar et al., 2003; Pagani et al., 2005; Jones et al., 2006; Wakana et al., 2007), and white matter templates (Mori et al., 2008). All of these approaches attempt to address the tissue specificity problem of VBA. The TBSS and tractography based approaches generally minimize the amount of spatial blurring that can be problematic with VBA methods. TBSS does this by creating a skeleton of tissues with high FA from normalized DTI data (Smith et al., 2006). The skeletons are then mapped back to the native DTI data for each subject and the DTI measurements are projected onto the skeleton. The skeleton approach is useful for defining WM regions with similar FA and will minimize the blurring of different tissues within the WM mask. The skeleton also reduces the number of multiple comparisons, which improves statistical power. The challenges with TBSS are related to the correspondence of the skeleton to specific WM anatomy, and how the data are projected onto the skeleton. WM tractography has also been applied to extract specific WM regions for quantitative analyses. Tractography offers the ability to obtain subject-specific tract regions-of-interest; however it is also prone to errors in the tensor orientation and crossing white matter fibers. Template based approaches are promising for extracting specific tissue regions; however, they require accurate coregistration between the template and the images being analyzed. A comparison of T-SPOON with these approaches, although potentially interesting, is beyond the scope of the current study.

In this study, we used a set of well-characterized DTI data comparing the microstructural properties of subjects with autism with age- and IQ-matched healthy controls. The main objective was to see if the observations in our previous region-of-interest studies of this data (Alexander et al., 2007a; Lee et al., 2007) were consistent with the results from a voxel-based analysis. It is clear that both the T-SPOON VBA and the UNSEG VBA resulted in significant regions that were similar to those that we explored with our previous hypothesis driven ROI studies. However, it is clear that although the T-SPOON and UNSEG results are similar, they are not identical. Even in the regions where the results are similar, T-SPOON removes the potential confounds of differential morphometry, which is critical for interpreting whether the group differences are caused by the DTI measures or the morphologic attributes of the brains and co-registration. These results suggested that both T-SPOON and UNSEG VBA were sensitive enough to identify regions that should be explored in further detail.

To date only a few other DTI studies of autism have been reported (Barnea-Goraly et al., 2004; Keller et al., 2007). Barnea-Goraly et al. (2004) performed a voxel-based group comparison study of FA in a small sample (7 children with autism and 9 controls) and reported decreased FA in autism for ventromedial prefrontal, anterior cingulate, corpus callosum, temporoparietal, superior temporal gyrus, temporal lobe and occipitotemporal regions. Keller et al. (2007) in a larger sample (34 autism and 31 controls — ages 10–35) found autism related reductions of FA in anterior cingulate, mid-body of the corpus callosum, right prefrontal, and right temporal–occipital regions. Our T-SPOON FA results show some similar region to these studies (corpus callosum, bilateral superior temporal gyrus WM, anterior cingulate regions) although there are differences in the results. The differences between the study results may be attributed to differences in the sample populations and analysis methods. Regardless, all of these studies implicate specific WM regions that warrant more detailed study. It is clear from the T-SPOON VBA results of the MD data in Fig. 7 that extensive WM regions may be implicated in autism. A more detailed analysis of autism DTI data described in the present study is being performed and will be the focus of a future publication.

Conclusions

The partial volume effects of spatial normalization and isotropic Gaussian kernel smoothing may be compensated in VBA by using a regional mask with the same smoothing parameters applied. The VBA of DTI data using T-SPOON generally appeared to be consistent with the statistical analysis of DTI data extracted from anatomical ROIs in the corpus callosum and temporal lobes. Future developments will focus on more accurate and robust anatomical registration and image region segmentation methods.

Acknowledgments

This work was supported by NIH Mental Retardation/Developmental Disabilities Research Center (MRDDRC — Waisman Center), NIMH 62015 (ALA), NIDA15879 (ALA), NIH P50 MH069315, NIMH RO1 MH080826 (JEL) an Autism Speaks Mentor-based Predoctoral Fellowship (JEL for MBD), NICHD U19 HD35476 (University of Utah CPEA), the Autism Society of Southwestern Wisconsin, and the National Alliance for Research in Schizophrenia and Affective Disorders (NARSAD — ML). We thank Andrew Fox, Terry Oakes, and Dan Kelley for stimulating

discussions and assistance with software implementation. We also thank Dr. Jeffrey Lu, Dr. William McMahon, Dr. Judith Miller, Michael Johnson, Jubel Morgan, Alyson Froehlich, Barbara Young, and the other staff of the Utah Autism Research Program and Henry Buswell, Melody Johnson, Dr. E.K. Jeong, and Dr. Dennis Parker of the University of Utah Center for Advanced Medical Technology for their assistance. We express our sincere gratitude to the children and adults who participated in this study and their families.

Disclaimer: The project described was supported by Grant Number RO1 MH080826 from the National Institutes Of Mental Health. The content is solely the responsibility of the authors and does not necessarily represent the official views of the National Institutes Of Mental Health or National Institutes of Health.

References

Albrecht, J., Dellani, P.R., Muller, M.J., Schermuly, I., Beck, M., Stoeter, P., Gerhard, A., Fellgiebel, A., 2007. Voxel based analyses of diffusion tensor imaging in Fabry disease. J. Neurol. Neurosurg. Psychiatry 78, 964–969.

Alexander, A.L., Hasan, K.M., Lazar, M., Tsuruda, J.S., Parker, D.L., 2001a. Analysis of partial volume effects in diffusion-tensor MRI. Magn. Reson. Med. 45, 770–780.

Alexander, D.C., Pierpaoli, C., Basser, P.J., Gee, J.C., 2001b. Spatial transformation of diffusion tensor magnetic resonance images. IEEE Trans. Med. Imaging 20 (11), 1131–1139.

Alexander, A.L., Lee, J.E., Lazar, M., Boudos, R., DuBray, M.B., Oakes, T.R., Miller, J.N., Lu, J., Jeong, E.K., McMahon, W.M., Bigler, E.D., Lainhart, J.E., 2007a. Diffusion tensor imaging of the corpus callosum in autism. NeuroImage 34, 61–73.

Alexander, A.L., Lee, J.E., Lazar, M., Field, A.S., 2007b. Diffusion tensor imaging of the brain. Neurotherapeutics 4, 316–329.

Ardekani, B.A., Guckemus, S., Bachman, A., Hoptman, M.J., Wojtaszek, M., Nierenberg, J., 2004. Quantitative comparison of algorithms for inter-subject registration of 3D volumetric brain MRI scans. J. Neurosci. Methods 142 (1), 67–76.

Ardekani, S., Kumar, A., Bartzokis, G., Sinha, U., 2007. Exploratory voxel-based analysis of diffusion indices and hemispheric asymmetry in normal aging. Magn. Reson. Imaging 25, 154–167.

Ashburner, J., Friston, K.J., 1999. Nonlinear spatial normalization using basis functions. Hum. Brain Mapp. 7 (4), 254–266.

Ashburner, J., Friston, K.J., 2000. Voxel-based morphometry, the methods. NeuroImage 11, 805–821.

Ashtari, M., Cervellione, K.L., Hasan, K.M., Wu, J., McIlree, C., Kester, H., Ardekani, B.A., Roofeh, D., Szeszko, P.R., Kumra, S., 2007. White matter development during late adolescence in healthy males: a cross-sectional diffusion tensor imaging study. NeuroImage 35 (2), 501–510.

Avants, B.B., Duda, J.T., Zhang, H., Gee, J.C., 2007. Multivariate normalization with symmetric diffeomorphisms for multivariate studies. Med. Image Comput. Comut. Assist. Interv. 10, 359–366.

Barnea-Goraly, N., Eliez, S., Hedeus, M., Menon, V., White, C.D., Moseley, M., Reiss, A.L., 2003. White matter tract alterations in fragile X syndrome: preliminary evidence from diffusion tensor imaging. Am. J. Med. Genet. B Neuropsychiatr. Genet. 118, 81–88.

Barnea-Goraly, N., Kwon, H., Menon, V., Stephan, E., Lotspeich, L., Reiss, A.L., 2004. White matter structure in autism: preliminary evidence from diffusion tensor imaging. Biol. Psychiatry 55 (3), 323–326.

Basser, P.J., Pierpaoli, C., 1996. Microstructural and physiological features of tissues elucidated by quantitative-diffusion-tensor MRI. J. Magn. Reson. 111, 209–219.

Basser, P.J., Mattiello, J., LeBihan, D., 1994. MR diffusion tensor spectroscopy and imaging. Biophys. J. 66 (1), 259–267.

Basser, P.J., Pajevic, S., Piepaoli, C., Duda, J., Aldroubi, A., 2000. In vivo fiber tractography using DT-MRI data. Magn. Reson. Med. 44, 625–632.

Berman, J.I., Mukherjee, P., Partridge, S.C., Miller, S.P., Ferriero, D.M., Barkovich, A.J., Vigneron, D.B., Henry, R.G., 2005. Quantitative diffusion tensor MRI fiber tractography of sensorimotor white matter development in premature infants. NeuroImage 27, 862–871.

Bonekamp, D., Nagae, L.M., Degaonka, M., Matsibm, M., Abdalla, W.M.A., Barker, P.B., Mori, S., Horska, A., 2007. Diffusion tensor imaging in children and adolescents: reproducibility hemispheric and age-related differences. NeuroImage 34, 733–742.

Borroni, B., Brambati, S.M., Agosti, C., Gipponi, S., Bellelli, G., Gasparotti, R., Garibotto, V., DiLuca, M., Scifo, P., Perani, D., Padovani, A., 2007. Evidence of white matter changes on diffusion tensor imaging in frontotemporal dementia. Arch. Neurol. 64 (2), 246–251.

Charlton, R.A., Barrick, T.R., McIntyre, D.J., Shen, Y., O, Sullivan, M., Howe, F.A., Clark, C.A., Morris, R.G., Markus, H.S., 2006. White matter damage on diffusion tensor imaging correlates with age-related cognitive decline. Neurology 66, 217–222.

Chappell, M.H., Ulu , A.M., Zhang, L., Heitger, M.H., Jordan, B.D., Zimmerman, R.D., Watts, R., 2006. Distribution of microstructural damage in the brains of professional boxers: a diffusion MRI study. J. Magn. Reson Imaging 24, 537–542.

Conturo, T.E., Lori, N.F., Cull, T.S., Akbudak, E., Snyder, A.Z., Shimony, J.S., Mckinstry, R.C., Burton, H., Raichle, M.E., 1999. Tracking neuronal fiber pathways in the living human brain. In Proc. Natl, Acad. Sci. USA 96, 10422–10427.

DaSilva, A.F.M., Granziera, C., Tuch, D.S., Snyder, J., Vincent, M., Hadjikhani, N., 2007. Interictal alterations of the trigeminal somatosensory pathway and periaqueductal gray matter in migraine. Neuroreport 18 (4), 301–305.

Grieve, S.M., Williams, L.M., Paul, R.H., Clark, C.R., Gordon, E., 2007. Cognitive aging, executive function, and fractional anisotropy: a diffusion tensor MR imaging study. AJNR Am. J. Neuroradiol. 28, 226–235.

Gupta, R.K., Saksena, S., Hasan, K.M., Agarwal, A., Haris, M., Pandey, C.M., Narayana, P. A., 2006. Focal Wallerian degeneration of the corpus callosum in large middle cerebral artery stroke: serial diffusion tensor imaging. J Magn. Reson. Imaging 24, 549–555.

Hubl, D., Koenig, T., Strik, W., Federspiel, A., Kreis, R., Boesch, C., Maier, S.E., Schroth, G., Lovblad, K., Dierks, T., 2004. Pathways that make voices: white matter changes in auditory hallucinations. Arch. Gen. Psychiatry 61 (7), 658–668.

Jenkinson, M., Smith, S.M., 2001. A global optimisation method for robust affine registration of brain images. Med. Image Anal. 5 (2), 143–156.

Jezzard, P., Balaban, R.S., 1995. Correction for geometric distortion in echo planar images from B0 field variations. Magn. Reson. Med. 34, 65–73.

Jones, D.K., Griffin, L.D., Alexander, D.C., Catani, M., Horsfield, M.A., Howard, R., Williams, S.C., 2002. Spatial normalization and averaging of diffusion tensor MRI data sets. Neuroimage 17, 592–617.

Jones, D.K., Symms, M.R., Cercignani, M., Howard, R.J., 2005. The effect of filter size on VBM analyses of DTI data. NeuroImage 26, 546–554.

Jones, D.K., Catani, M., Pierpaoli, C., Reeves, S.J.C., Shergill, S.S., O, Sullivan, M., Golesworthy, P., McGuire, P., Horsfield, M.A., Simmons, A., Williams, S.C.R., Howard, R.J., 2006. Age effects on diffusion tensor magnetic resonance imaging tractography measures of frontal cortex connections in schizophrenia. Hum. Brain Mapp. 27, 230–238.

Jones, D.K., Chitnis, X.A., Job, D., Khong, P.L., Leung, L.T., Marenco, S., Smith, S.M., Symms, M.R., 2007. What happens when nine different groups analyze the same DT-MRI data using voxel-based methods? Proceedings of the 15th Annual ISMRM Meeting. Berlin, Germany, p. 74.

Kanaan, R.A., Shergill, S.S., Barker, G.J., Catani, M., Ng, V.W., Howard, R., McGuire, P.K., Jones, D.K., 2006. Tract-specific anisotropy measurements in diffusion tensor imaging. Psychiatry Research; Neuroimaging 146 (1), 73–82.

Keller, T.A., Kana, R.K., Just, M.A., 2007. A developmental study of the structural integrity of white matter in autism. Neuroreport 18 (1), 23–27.

Kubicki, M., Shenton, M.E., Salisbury, D.F., Hirayasu, Y., Kasai, K., Kikinis, R., Jolesz, F.A., McCarley, R.W., 2002. Voxel-based morphometric analysis of gray matter in first episode schizophrenia. NeuroImage 17, 1711–1719.

Kumra, S., Ashtari, M., Cervellione, K.L., Henderson, I., Kester, H., Roofeh, D., Wu, J., Clarke, T., Thaden, E., Kane, J.M., Rhinewine, J., Lencz, T., Diamond, A., Ardekani, B.A., Szeszko, P.R., 2005. White matter abnormalities in early-onset schizophrenia: a voxel-based diffusion tensor imaging study. J. Am. Acad Child Adolesc. Psychiatry 44 (9), 934–941.

Lazar, M., Weinstein, D.M., Tsuruda, J.S., Hasan, K.M., Arfanakis, K., Meyerand, M.E., Badie, B., Rowley, H.A., Haughton, V., Field, A., Alexander, A.L., 2003. White matter tractography using diffusion tensor deflection. Hum. Brain Mapp. 18, 306–321.

Lee, J.E., Bigler, E.D., Alexander, A.L., Lazar, M., DuBray, M.B., Chung, M.K., Johnson, M., Morgan, J., Miller, J.N., McMahon, W.M., Lu, J., Jeong, E.K., Lainhart, J.E., 2007. Diffusion tensor imaging of white matter in the superior temporal gyrus and temporal stem in autism. Neurosci. Lett. 424 (2), 127–132.

Mori, S., Oishi K., Jiang, H., Jiang, L., Li, X., Akhter, K., Hua, K., Faria, A.V., Mahmood, A., Woods, R., Toga, A.W., Pike, G.B., Neto, P.R., Evans, A., Zhang, J., Huang, H., Miller, M.I., van Zijl, P., Mazziotta, J., 2008. Stereotaxic white matter atlas based on diffusion tensor imaging in an ICBM template. NeuroImage 40, 570–582.

Oakes, T.R., Fox, A.S., Johnstone, T., Chung, M.K., Kalin, N., Davidson, R.J., 2007. Integrating VBM into the general linear model with voxelwise anatomical covariates. NeuroImage 34, 500–508.

Pagani, E., Filippi, M., Rocca, M.A., Horsfield, M.A., 2005. A method for obtaining tract-specific diffusion tensor MRI measurements in the presence of disease: application to patients with clinically isolated syndromes suggestive of multiple sclerosis. NeuroImage 26, 258–265.

Park, H.J., Kubicki, M., Shenton, M.E., Guimond, A., McCarley, R.W., Majer, S.E., Kikinis, R., Jolesz, F.A., Westin, C.F., 2003. Spatial normalization of diffusion tensor MRI using multiple channels. NeuroImage 20 (4), 1995–2009.

Park, H.J., Westin, C.F., Kubicki, M., Majer, S.E., Niznikiewicz, M., Baer, A., Frumin, M., Kikinis, R., Jolesz, F.A., McCarley, R.W., Shenton, M.E., 2004. White matter hemisphere asymmetries in healthy subjects and in schizophrenia: a diffusion tensor MRI study. NeuroImage 23 (1), 213–223.

Paus, T., Zijdenbos, A., Worsley, K., Collins, D.L., Blumenthal, J., Giedd, J.N., Rapoport, J.L., Evans, A.C., 1999. Structural maturation of neural pathways in children and adolescents: in vivo study. Science 283, 1908–1911.

Salat, D.H., Tuch, D.S., Greve, D.N., van der Kouwe, A.J., Hevelone, N.D., Zaleta, A.K., Rosen, B.R., Fischl, B., Corkin, S., Rosas, H.D., Dale, A.M., 2005. Age-related alterations in white matter microstructure measured by diffusion tensor imaging. Neurobiol. Aging 26 (8), 1215–1227.

Schmithorst, V., Wilke, M., 2002. Differences in white matter architecture between musicians and non-musicians: a diffusion tensor imaging study. Neurosci. Lett. 321 (1–2), 57–60.

Schmithorst, V., Wilke, M., Dardzinski, B.J., Holland, S.K., 2002. Correlation of white matter diffusivity and anisotropy with age during childhood and adolescence: a cross-sectional diffusion-tensor MR imaging study. Radiology 222 (1), 212–218.

Smith, S.M., Jenkinson, M., Johansen-Berg, H., Rueckert, D., Nichols, T.E., Mackay, C.E., Watkins, K.E., Ciccarelli, O., Zaheer Cader, M., Matthews, P.M., Behrens, E.J.T., 2006.

Tract-based spatial statistics: voxelwise analysis of multi-subject diffusion data. NeuroImage 31, 1487–1505.
Snook, L., Plewes, C., Beaulieu, C., 2007. Voxel based versus region of interest analysis in diffusion tensor imaging of neurodevelopment. NeuroImage 34, 243–252.
Tuch, D.S., Salat, D.H., Wisco, J.J., Zaleta, A.K., Hevelone, N.D., Rosas, H.D., 2005. Choice reaction time performance correlates with diffusion anisotropy in white matter pathways supporting visuospatial attention. Proc. Natl. Acad Sci. U. S. A. 102 (34), 12212–12217.
Wakana, S., Caprihan, A., Panzenboeck, M.M., Fallon, J.H., Perry, M., Gollub, R.L., Hua, K., Zhang, J., Jiang, H., Dubey, P., Blitz, A., van Zijl, P., Mori, S., 2007. NeuroImage 36, 630–644.
Whitcher, B., Wisco, J.J., Hadjikhani, N., Tuch, D.S., 2007. Statistical group comparison of diffusion tensors via multivariate hypothesis testing. Magn. Reson. Med. 57 (6), 1065–1074.
Woods, R.P., Grafton, S.T., Holmes, C.J., Cherry, S.R., Mazziotta, J.C., 1998. Automated image registration: I. General methods and intrasubject, intramodality validation. J. Comput. Assist. Tomogr. 22, 139–152.
Xu, D., Mori, S., Shen, D., van Zijl, P.C.M., Davatzikos, C., 2003. Spatial normalization of diffusion tensor fields. Magn. Reson. Med. 50, 175–182.
Xu, J., Rasmussen, I.A., Lagopoulos, J., Haberg, A., 2007. Diffuse axonal injury in severe traumatic brain injury visualized using high-resolution diffusion tensor imaging. J. Neurotrauma 24 (5), 753–765.
Xue, R., van Zijl, P.C.M., Crain, B.J., Solaiyappan, M., Mori, S., 1999. In vivo three-dimensional reconstruction of rat brain axonal projections by diffusion tensor imaging. Magn. Reson. Med. 42, 1123–1127.
Zhang, Y., Brady, M., Smith, S., 2001. Segmentation of brain MR images through a hidden markov random field model and the expectation–maximization algorithm. IEEE Trans. Med. Imag. 20, 45–57.
Zhang, H., Yushkevich, P.A., Alexander, D.C., Gee, J.C., 2006. Deformable registration of diffusion tensor MR images with explicit orientation optimization. Med. Image Anal. 10 (5), 764–785.